CHAPTER IX

FISCHER-TROPSCH SYNTHESIS: OXIDATION OF A FRACTION OF COBALT CRYSTALLITES IN RESEARCH CATALYSTS AT THE ONSET OF FT AT PARTIAL PRESSURE MIMICKING 50% CO CONVERSION

9.1 Abstract

Freshly H_2-reduced cobalt catalyst samples and FTS catalyst samples (i.e., freshly reduced and immediately exposed to the onset of FTS conditions corresponding to 50% CO conversion) were prepared. Each sample was coated in-situ using molten polywax and solidified so that an air-protected sample was obtained, which was stored in inert gas. XAS was utilized to investigate the oxidation state of cobalt. A fraction of cobalt crystallites in the freshly reduced research catalysts having lower-than-commercial loading and smaller crystallites undergoes a degree of oxidation to CoO at the onset of FTS conditions simulating 50% CO conversion (i.e., the H_2O partial pressure is high enough to induce some oxidation). Therefore, by decreasing Co content with the aim of improving the dispersion of cobalt and Co efficiency, very small Co crystallites are obtained. Their reoxidation at the onset of FTS is an unintended consequence. Thus, catalysts should be designed to have an optimum narrow cluster size range — small enough to increase Co surface site densities, but large enough to avoid reoxidation, and the stability problems that arise from having unreduced Co in the working catalyst (e.g., a complex coalescence and reduction mechanism).

Keywords: Fischer-Tropsch synthesis (FTS), gas-to-liquids (GTL), cobalt crystallites, size-dependent reoxidation

9.2 Introduction

Improving the stability of Co/Al_2O_3 catalysts for Fischer-Tropsch synthesis (FTS) is an important challenge facing the commercial development of these catalysts for the conversion of coal, biomass, and natural gas to liquid fuels as alternative resources to crude oil (Jacobs et al., 2002). There is a debate regarding whether small cobalt nanoparticles oxidize under realistic synthesis conditions (Tsakoumis et al., 2010). Part of the confusion stems from the fact that while some groups are examining commercial catalysts using high cobalt loadings to stabilize against reoxidation, other groups employ research catalysts aimed at reducing the amount of expensive cobalt metal and improving Co efficiency. Another major source of confusion has to do with the time period under which catalysts are examined, and the definition of "initial deactivation". While some groups examine the decay period prior to leveling off for realistic commercial catalysts under relevant FTS conditions, others have focused on the susceptibility of small cobalt crystallites at the onset of FTS - i.e., when the freshly activated catalyst is exposed to realistic FTS conditions or conditions that mimic them.

Typically, a slurry impregnation method is employed to prepare Co/alumina catalysts having higher loadings, while incipient wetness impregnation (IWI) is often used to prepare Co catalysts with lower loadings. The slurry impregnation method tends to produces larger Co clusters (~8-15 nm by (Jacobs et al., 2002)) at 15-25%Co loadings on γ-Al_2O_3. With the IWI method, average size is sensitive to loading (~5 nm at 15%Co and ~10-15 nm clusters at 25%Co). With an average cluster size of ~5 nm, there exists a fraction of particles < (2 - 4 nm) that could undergo reoxidation as suggested by recent thermodynamics calculations (Van Steen et al., 2005). TPR profiles for Co/Al_2O_3 catalysts show broadened peaks for the CoO reduction step suggesting a distribution of sizes. Thus, reoxidation of a fraction of Co^0 crystallites to CoO is important to assess. Another possibility is reaction of small Co^0 crystallites with the support (Jacobs et al., 2003; Sirijaruphan et al., 2003) (via CoO intermediate).

Cobalt support compounds also form from reaction of residual CoO from incomplete reduction, due to strong interactions with Al_2O_3. Moodley et al.

(Moodley et al., 2011) examined used catalyst samples from a CSTR. By adjusting CO conversion and P(tot) to achieve $P(H_2O)$ = 10 bar, ~10% cobalt aluminate was identified and attributed to the conversion of residual CoO (from incomplete reduction). There is the possibility that a fraction of the $CoAl_2O_4$ identified in used catalyst samples from our group (Das et al., 2003; Jacobs et al., 2002) came from CoO resulting from incomplete reduction. A used unpromoted 15%Co/Al_2O_3 catalyst (with half the % reduction of promoted catalysts) had 2 to 3 times the amount of cobalt aluminate compared to used Pt and Ru promoted 15%Co/Al_2O_3 catalysts (Jacobs et al., 2002). Transforming from CoO to $CoAl_2O_4$ retains the Co^{2+} state, but $CoAl_2O_4$ is more difficult to reduce.

In the initial decay period of FTS, net oxidation of Co is typically not observed. Investigating used 0.2%Re-15%Co/Al_2O_3 catalyst samples periodically withdrawn from a CSTR reactor as a function of time, XAS analysis (Das et al., 2003; Jacobs et al., 2006) demonstrated that considerable CoO was present initially, as peaks were present for Co-O and Co-Co in the oxide in EXAFS spectra (Das et al., 2003). As the catalyst underwent initial deactivation and leveling off, the extent of Co reduction increased slowly with time on stream (Jacobs, et al., 2006), Co-Co coordination increased to suggest possible sintering (Das et al., 2003), and a small amount of cobalt aluminate was formed (Das et al., 2003). During the run, there was a slow decrease in the white line intensity (increasing extent of Co reduction) (Jacobs et al., 2006) and a significant growth in the Co-Co coordination metal shell (Das et al., 2003). The main point is that while net oxidation during the initial decay period as a function of time on-stream was not observed by us, any CoO present in the working catalyst may coalesce to form larger domains that undergo reduction during FT. Co particles present may also agglomerate or ripen, a process that could be exacerbated by any additional Co0 formed from net slow reduction of sintered CoO during the course of a run. The groups of van Steen, Claeys et al. (Van Steen, 2011) have recently confirmed sintering of Co with time on-stream during the initial decay period using a magnetometer. The susceptibility of Co in a Pt promoted Co/Al_2O_3 catalyst to oxidation in a commercial catalyst run in a 100 barrel/day slurry bubble column reactor was explored by Saib et al. (Saib et al., 2006; Van de Loosdrecht et al., 2007). A decreasing white line intensity in XANES spectra as a function of time

was observed, suggesting that the decay period was not due to Co reoxidation. Average crystallite (i.e., not cluster) size was 6 nm, above the 4.4 nm threshold, below which van Steen et al. (Van Steen, et al., 2005) have indicated oxidation may occur.

However, it is also important to examine one other region of deactivation, and that is the onset of FTS when a freshly activated catalyst is directly exposed to high conversion FTS conditions (i.e., immediately before the decay period). By a linear extrapolation to time zero, it is intriguing that only 35% cobalt reduction was obtained for our 0.2%Re-15%Co/Al_2O_3 catalyst (Jacobs et al., 2006) at the onset of FTS while it should have been 55% (Das et al., 2003) as measured for the freshly activated catalyst. The results suggest that some reoxidation of small crystallites may have occurred at the onset of FTS. The average cluster (i.e., cluster of smaller crystallites) size was ~5 nm.

The sensitivity of Co catalysts to H_2O has been explored by many research groups (Jacobs et al., 2004; Li et al., 2002; Li et al., 2002; Saib et al., 2010; Storsater et al., 2005), as water is often cited as exacerbating deactivation. For a 0.5%Pt-15%Co/Al_2O_3 catalyst having an average Co cluster size of ca. 5.6 nm, replacing inert balancing gas by 28% by volume H_2O led to catastrophic irreversible deactivation (Storsater et al., 2005); formation of cobalt support compounds (e.g., cobalt aluminate) was identified in XANES derivative spectra (Jacobs et al., 2003). An unpromoted catalyst containing a higher Co loading (25%Co with cobalt cluster size ca.12 nm) was found to be much more robust (Van Steen, 2011). The catalyst displayed metallic character prior to (and following) 25%H_2O addition, but during 25%H_2O addition some CoO formation was observed in the XANES spectra (Van Steen, 2011), and the catalyst largely recovered its activity. Increasing Co cluster size was deemed beneficial for stabilizing the catalyst against deactivation.

The group of Claeys obtained results using a magnetometer and XRD revealing that smaller Co crystallites oxidize more readily than larger ones during FTS at useful conversions (Feltes et al., 2013; Fischer et al., 2012). A drop in magnetization with increasing water partial pressure was most evident at >60% simulated conversions, due to re-oxidation of small crystallites within the overall size distribution (Feltes et al., 2013; Fischer et al., 2012). Recently, another study

reported reoxidation (using XANES) of a Ru-Co/Al_2O_3 catalyst after an excursion to high conversion, and increases in CO_2 and CH_4 selectivities were observed (Ma et al., 2011). An investigation using both in-situ synchrotron XRD and XANES to follow both activation and catalyst stability during FTS for a 1%Re-20%Co/γ-Al_2O_3 catalyst with an average Co crystallite size of 10.7 nm (as measured by XRD), the catalyst was found to maintain its oxidation state and particle size during 6 h of reaction (conditions: 210 °C, 18 bar, 30 – 50% CO conversion, H_2:CO ratio of 2:1) (Rønning et al., 2010). Again, a larger size seems beneficial from the standpoint of stability.

There is reasonable evidence to suggest that, as a function of time on-stream, CoO continues to agglomerate, reduce, and, consequently, ripen into larger Co0 metal particles during initial catalyst deactivation prior to the longer term leveling off period. However, the sources of CoO remain unclear. That is, does CoO form from the oxidation of small Co crystallites in research catalysts with high dispersion upon exposure to FTS conditions at useful conversions, or is the presence of CoO in the working catalyst solely from incomplete activation? We and others (Das et al., 2003; Jacobs et al., 2002; Moodley et al., 2011) have also observed by XANES that a fraction of cobalt in used samples is due to cobalt support compound formation. The question remains as to the original source of this species – is it solely due to unreduced CoO following activation that reacts with the support, or can small Co0 crystallites oxidize at the onset of reaction to CoO, and in turn react with the support? We intend to shed light on these points. Catalysts were prepared with low Co loading with the aim of deliberately preparing a small Co cluster size,and freshly reduced catalyst samples were then exposed to FT conditions simulating 50% CO conversion. XANES/EXAFS were used to assess whether any change in Co oxidation state occurred. The effects of Co loading, Pt promoter, and support on the reoxidation of cobalt at the onset of FTS conditions were explored.

9.3 Experimental

9.3.1 Catalyst Preparation and Sample Preparation

Alumina (Catalox 200 γ-Al_2O_3) and granular activated carbon (Calgon) were utilized as catalyst support materials in this work. They were first calcined to remove physisorbed water before use. Alumina was calcined at 400 °C in a muffle furnace, while Calgon carbon was calcined under flow of nitrogen at 350 °C in order to avoid the oxidation of carbon during calcination. The catalysts were prepared using incipient wetness impregnation (IWI) with cobalt nitrate as the precursor. Deionized water was used to prepare a cobalt nitrate solution for Co/Al_2O_3, while acetone was utilized to prepare a cobalt nitrate solution for the Co/Calgon carbon catalyst. For Co/Al_2O_3, cobalt loadings of 2%, 5%, and 10% were prepared. To obtain 10%Co on Al_2O_3, two impregnation steps were required with drying at 95 °C under vacuum in a rotary evaporator after each impregnation. For Co/Calgon carbon catalyst, only 2% Co on Calgon carbon was prepared and multiple impregnation steps were necessary due to the solubility limit of cobalt nitrate in acetone. After each impregnation step, the catalyst was dried under vacuum using a rotary evaporator. To prepare the 0.5% by weight Pt-promoted catalyst, either tetra-amine platinum (II) nitrate solution or platinum (II) acetylacetonate powder was utilized. Platinum was added by incipient wetness impregnation (IWI), after the last cobalt impregnation step. In the case of the Pt promoted Co/Al_2O_3 catalyst, tetra-amine platinum (II) nitrate solution was used as the platinum source. For Pt promoted Co/Calgon carbon, platinum (II) acetylacetonate was used. Multiple impregnation steps were also required in the case of Co/Calgon carbon catalyst, as platinum (II) acetylacetonate only slightly dissolves in acetone. Finally, all catalysts were calcined under different conditions depending on the nature of each catalyst support; i.e., Co/Al_2O_3 and Pt-Co/Al_2O_3 catalysts were calcined under a flow of air at 350 °C for 4 h, while Pt-Co/Calgon carbon catalyst was calcined under flowing nitrogen at 350 °C for 4 h.

To prepare a reduced sample, each catalyst was pressed into a flat pellet inside a 1" I.D. reactor with boron nitride. 80 sccm flow of H_2 was started. The reactor was slowly (100 °C/h) brought up to an activation temperature of 400°C

for Pt-Co/Al_2O_3, 550 °C for Co/Al_2O_3, or 500 °C for Co/Calgon carbon, and held for 12 h. A separate steel tube was filled with Polywax 725 at 1 atm and brought up to 200 °C under N_2 flow (20 sccm). The reactor was cooled to 220 °C and held at this temperature. Next, the reactor was closed and H_2 flow was stopped, flow to the reactor containing the polywax was reversed and the polywax was pushed into the reactor containing the cobalt catalyst to encapsulate the pellet in polywax and prevent oxidation from occurring.

The same initial reduction conditions were repeated for each of the Co catalysts in preparation of the FTS samples. Once the reactor was cooled to 220 °C, the reactor was slowly pressurized to 300 psig using 100 sccm of N_2. The reactor was then bypassed, and a flow of 100 sccm CO, 200 sccm H_2 and, 100 sccm H_2O (g) was set to mimic partial pressures at 50% conversion. After a 90 min period, the water, CO and H_2 gases were shut off, and N_2 at 20 sccm was allowed to enter. The inlet line was immediately bypassed to prevent any excess water from passing through the reactor. The reactor was slowly depressurized for polywax encapsulation, and the sample was stored in inert gas for EXAFS/XANES analysis.

9.3.2 BET Surface Area and Porosity Measurement

Brunauer, Emmett, and Teller (BET) (Brunauer et al., 1938) and Barrett, Joyner, and Halenda (BJH (Barrett et al., 1951)) measurements for both supports and calcined catalysts were carried out using a Micromeritics Tri-Star system. Prior to adsorption measurements, samples were gradually ramped to 160 °C and evacuated to approximately 50 mTorr for 12 h.

9.3.3 Temperature Programmed Reduction (TPR)

Temperature programmed reduction (TPR) profiles of calcined catalysts were recorded using a Zeton-Altamira AMI-200 unit equipped with a thermal conductivity detector (TCD). Samples were pretreated by purging with argon flow at 350 °C to remove traces of water. The TPR was performed using a 10%H_2/Ar gas mixture (referenced to argon) at a flow rate of 30 cm^3/min. The catalyst samples were heated from 50 to 1100 °C. In the case of Co/Calgon carbon,

an upper temperature limit of 800 °C was set due to the degradation of Calgon carbon at higher temperature.

9.3.4 Hydrogen Chemisorption and Oxygen Pulse Reoxidation

Hydrogen chemisorption was conducted using temperature programmed desorption (TPD), also measured with a Zeton-Altamira AMI-200 instrument. The sample weight was typically ~0.220 g. Catalysts were activated using a 1:2 H_2/Ar mixture at a total flow rate of 30 cm^3/min at different reduction temperatures (i.e., 400 °C for Pt-Co/Al_2O_3, 550 °C for Co/Al_2O_3, and 500 °C for Co/Calgon carbon) for 10 h and, then, cooled to 100 °C under flowing H_2. The catalyst sample was held at 100 °C and purged with argon to remove and/or prevent adsorption of weakly bound hydrogen species prior to increasing the temperature slowly to the activation temperature of each catalyst (e.g., 400 °C, 500 °C, or 550 °C, respectively). At that temperature, the sample was held under flowing argon to desorb any remaining chemisorbed hydrogen until the TCD signal returned to the baseline. The TPD spectrum was integrated and the number of moles of hydrogen desorbed was determined by comparing its area against the area of calibrated hydrogen pulses. The loop volume was first determined by establishing a calibration curve with syringe injections of hydrogen in helium flow. Uncorrected Co cluster size was calculated by ignoring the percentage of Co reduction, with the assumption of a 1:1 H:Co stoichiometric ratio and a spherical cobalt cluster morphology, respectively. After TPD of hydrogen, the sample was reoxidized at the activation temperature using pulses of oxygen in helium. After oxidation of the cobalt metal clusters, the number of moles of oxygen consumed was determined, and the percentage of reduction was calculated by assuming that the Co0reoxidized to Co_3O_4. By including the percentage of Co reduced in the calculation, the corrected Co cluster size was obtained. Further details of the procedure are provided elsewhere (Jacobs et al., 2002). There is, however, an exception in the case of the Co/Calgon carbon catalyst. The oxygen pulse reoxidation experiment was not possible because Calgon carbon material oxidized under oxygen pulses at high temperature. For that case, only uncorrected Co cluster size is reported. In addition, the contribution of Pt to the chemisorption data was neglected. Previous EXAFS

experiments confirmed that Pt is associated with Co at the atomic level, with no Pt-Pt bonds being detected even at Co/Pt ratios as low as 9 (Guczi et al., 2002). Here, the worst case scenario is that of the 0.5%Pt-2%Co catalysts, but even for that case the Co/Pt ratios are high and greater than 13. Thus, it is assumed that Pt is incorporated into the Co particles (i.e., considering that only Pt-Co bonding has only been observed previously by EXAFS), and thus its contribution to the metal site density was assumed to be very minor.

9.3.5 X-ray Absorption Near Edge Structure and Extended X-ray Absorption Fine Structure (XANES/EXAFS)

XAS measurements on catalysts as well as references were conducted at the National Synchrotron Light Source (NSLS) at Brookhaven National Laboratory (beamline X-18b), Upton, New York. Some preliminary measurements were also conducted at Argonne National Laboratory's Advanced Photon Source. The beamline at NSLS was equipped with a Si(111) channel-cut monochromator. A crystal detuning procedure was employed to prevent glitches arising from harmonics. The second crystal of the channel-cut monochromator is weakly linked to the crystal and slightly spring loaded. The other side is a picomotor, a very fine high-pitch screw that turns by piezo, which allows for slight detuning of the crystal. The X-ray ring at the NSLS has a flux of 1×10^{10} photons s^{-1} at 100 mA and 2.5 GeV, and the energy-range capability at X18b is 5.8-40 keV. All catalyst samples were prepared at CAER in the form of catalyst particles embedded in polywax (i.e., with storage in inert gas) as previously described. XANES/EXAFS spectra were recorded at the cobalt K-edge (7.709 keV) in transmission mode and a Co metallic foil spectrum was measured simultaneously with each sample spectrum for the purpose of energy calibration.

XANES spectra were processed using the WinXAS program. A simultaneous pre- and post-edge background removal step was carried out using 2 polynomials (degree 2) over the ranges 7.63-7.67 and 7.79-8.68 keV, respectively, and the resulting spectra were normalized by dividing by the height of the absorption edge. Normalized XANES spectra were compared with those of references. In addition to a bulk CoO reference compound spectrum, a catalyst spectrum

representing CoO in 15%Co/Al_2O_3 catalyst (i.e., from a TPR-XANES run previously conducted at Argonne (Jacobs et al., 2007)) was also used as a reference spectrum, as it is a more relevant reference spectrum for investigating CoO formation in the working Co/Al_2O_3 catalyst. XANES spectra of both reduced and FTS samples of each catalyst were directly compared in order to determine whether the freshly reduced Co^0 undergoes any oxidation at the onset of FTS.

Data reduction of EXAFS spectra was also performed using WinXAS. Following the normalization procedure previously described, spectra were converted to k-space and a k weighting of 1 was used. An advanced cubic weighted spline over 3 sections of the 2-14 $Å^{-1}$ range was used to remove the background of the $\chi(k)$ function. Finally, the k1-weighted results were Fourier transformed to R-space using a Bessel window. To quantify the changes in Co-O and Co-Co coordination number, fitting of the spectra in k space was carried out using FEFFIT. The k-range used was from 2 to 14 $Å^{-1}$. Theoretical EXAFS were generated using FEFF for model cobalt metal and CoO crystal parameters generated by ATOMS. In order to use coordination number as a fitting parameter, S_0^2 was assumed to be 0.9 by the zeroth order approximation. The other fitting parameters utilized by FEFFIT included the overall E_0 shift e_0 applied to each path, an isotropic expansion coefficient α which is multiplied by the nominal length of each path, and the Debye-Waller factor, σ^2.

9.4 Results and Discussion

9.4.1 BET Surface Area and Porosity Measurements

The results of surface area and porosity data measured by N_2 adsorption-desorption at 77 K are shown in Table 9.1. The γ-alumina support is a mesoporous material (2 nm < D < 50 nm) and activated Calgon carbon is a microporous material (D < 2 nm), and the results of BET measurements confirm these characteristics. In comparison, the BET surface area of Calgon carbon is fivefold higher than that of alumina, while the average pore diameter is one-fifth that of alumina. Considering the Co/Al_2O_3 catalysts, at low cobalt loading (2, 5%) the effect of cobalt oxide on surface area of alumina support is not significant, as expected, but a decrease was observed at the higher loading of 10%Co. However, although a drop in surface area was obtained, it

is still higher than the expected calculated value; that is, a 10%Co/Al_2O_3 catalyst corresponds to 13.6 % by weight of Co_3O_4. Assuming that Al_2O_3 is the only contributor to the surface area, then the area of 10%Co/Al_2O_3 catalyst should be $0.8638 \times 197 = 170$ m^2/g. The measured value is 181.9 m^2/g, so pore blocking is not deemed to be a significant issue. Adding 0.5%Pt promoter to Co/Al_2O_3 did not measurably change the BET surface area and porosity properties of the Co/Al_2O_3 catalysts. For 0.5%Pt-2%Co/Calgon carbon, no significant changes in BET surface area and porosity properties were observed compared to those of the Calgon carbon support.

Table 9.1 The results of BET surface area and porosity measurements and H_2 chemisorption/O_2 pulse reoxidation results of supports and catalysts

Catalyst	BET SA, m^2/g	Pore vol. (single point), cm^3/g	Avg. pore rad., nm	Reduced T (°C)	H_2 desorbed per g_{cat}, µmol/g	Uncorr. Co avg. diam., nm	O_2 uptake per g_{cat}, µmol/g	% Red. of Co	Corr. Co avg. diam., nm
Catalox 200 γ-Al_2O_3	197	0.473	5.0	-	-	-	-	-	-
Calgon carbon	1102	0.583	1.1	-	-	-	-	-	-
0.5%Pt -2%Co/Al_2O_3	208	0.438	4.2	400	78	2.3	35	16	0.4
0.5%Pt- 5%Co/Al_2O_3	200	0.425	4.4	400	79	5.5	342	61	3.4
0.5%Pt-10%Co/Al_2O_3	180	0.369	4.3	400	115	7.6	792	70	5.3
2%Co/Al_2O_3	208	0.444	4.3	550	32	5.4	20	9	0.5
5%Co/Al_2O_3	199	0.414	4.2	550	43	10.2	278	49	5.0
10%Co/Al_2O_3	182	0.374	4.1	550	80	11.0	656	58	6.4
0.5%Pt-2%Co/Calgon carbon*	1005	0.534	1.1	500	43	4.1	-	-	-

*O_2 pulse reoxidation cannot be applied for Co/Calgon carbon catalyst due to oxidation of Calgon carbon support.

9.4.2 Catalyst Reducibility

Figure 9.1 shows the TPR profiles of all catalysts. Considering unpromoted 5% and 10%Co/Al_2O_3 catalysts, their TPR profiles contain 4 major peaks; the first peak (~270 °C) and the second broad peak (~500 °C) are typically due to $Co_3O_4 \rightarrow CoO$ and $CoO \rightarrow Co^0$, respectively (Jacobs et al., 2007), and the third peak (~ 670 °C) appearing as a shoulder of the second peak is likely a very small CoO species interacting with the support. The fourth peak at high temperature (960 °C for 5%Co and 920 °C for 10%Co) is attributed to the decomposition of $CoAl_2O_4$ (Wang et al., 1991). In 2%Co/Al_2O_3, only two peaks are present at 260 °C and 990 °C. The first one represents the transformation of Co_3O_4 to CoO and the one at high temperature indicates the presence of $CoAl_2O_4$, perhaps suggesting that a fraction of the CoO formed reacted with Al_2O_3. Interestingly, at 2%Co loading, H_2 reduction does not successfully produce an adequate fraction of Co metal due to the strong interaction between Co and the alumina support. However, at higher loadings of 5% and 10%Co, the Co content is high enough to weaken the support interaction, thus allowing for a useful fraction of Co metal to be formed. Pt promoter improved the reducibility of cobalt oxides (Guczi et al., 2002; Jacobs et al., 2004; Jacobs et al., 2002; Jacobs et al., 2002; Li et al., 2002). Although Pt enhances the reduction of Co_3O_4 to CoO in 2%Co/Al_2O_3, the second peak of $CoAl_2O_4$ still remained and appears at nearly the same temperature as that of the unpromoted catalyst (990 °C). Nevertheless, for this very low Co loading catalyst, chemisorption results indicate that a small fraction of CoO does reduce and form highly dispersed Co^0, while it also appears that a fraction of CoO reacts with the support, contributing to the $CoAl_2O_4$ peak in TPR. For Pt promoted 2%Co/Calgon, its TPR profile also shows the progression of Co_3O_4 and CoO reduction with increasing reduction temperature. Overlapping of the reduction peaks indicates that CoO generated from the first step of reduction promptly continues to be reduced to Co metal. Note that the profile for this catalyst does not proceed beyond 800 °C due to reaction of the Calgon carbon support material; however, it is not necessary to proceed to higher temperatures since the peaks of interest fall within the desired range of the TPR temperatures selected. Some decomposition of the support below 600 °C, perhaps due to thermal decomposition of oxygenate groups, cannot be ruled out. Interestingly, the addition

of Pt did not shift the peaks to the same extent as observed with the cobalt/alumina catalysts. This may be due to interaction between cobalt and oxygenate groups on the ultra-high surface area support or porous effects. Nevertheless, one advantage of utilizing carbon was the apparent lack of formation of cobalt support compounds (which was observed in the case of alumina supported cobalt). This is evident from the high degree of reduction observed in XANES spectra (to be discussed).

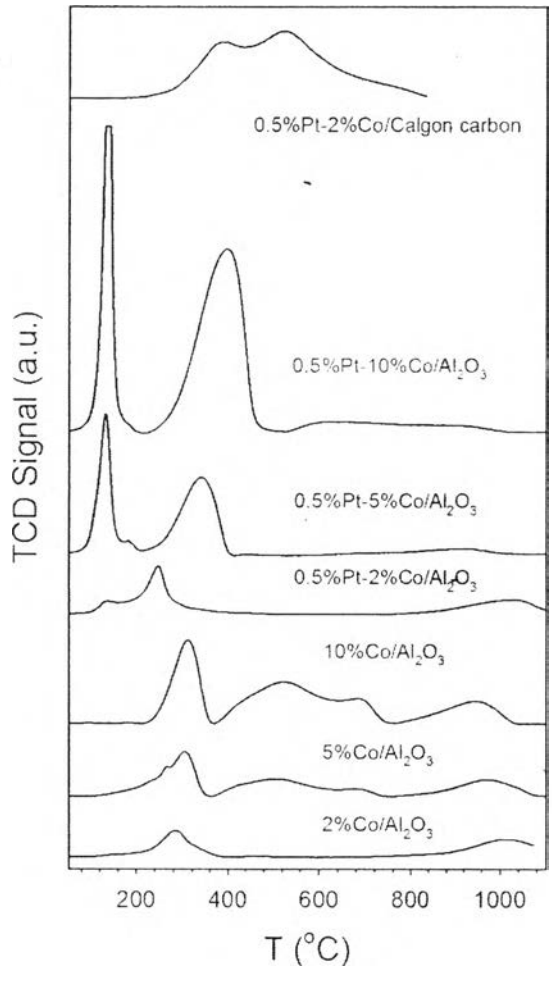

Figure 9.1 Comparative TPR spectra of unpromoted Co/Al_2O_3 catalysts, Pt promoted Co/Al_2O_3catalysts, and Pt promoted Co/Calgon carbon catalyst.

9.4.3 Cobalt Site Density and Size

Hydrogen chemisorption and oxygen pulse reoxidation results are tabulated in Table 9.1. The reduction temperature applied to each catalyst was based on the TPR results in Figure 9.1 (e.g., 400 °C for Pt promoted Co/Al_2O_3, 500 °C for Pt promoted Co/Calgon, and 550 °C for unpromoted Co/Al_2O_3). As expected, the % reduction of cobalt oxide and Co dispersion were improved in Co/Al_2O_3 catalysts after adding the Pt promoter. The Co cluster size decreased slightly in Pt promoted 5% and 10%Co/Al_2O_3 compared with those of unpromoted catalysts at the same Co contents. This is likely due to the fact that Pt assists in reducing more strongly interacting species, which tend to be smaller. At a low Co loading of 2%, there is no significant change in Co cluster size (0.5 vs 0.4 nm) after adding Pt promoter in spite of an increase in % reduction. Moving to Pt promoted Co/Calgon carbon catalyst, although percentage cobalt oxide reduction and corrected Co cluster size cannot be estimated, the uncorrected values provide an upper limit to average Co diameter. With the aim of this work being to investigate the susceptibility of small cobalt crystallites to reoxidation at the onset of FT reaction at 50% CO conversion, these activation temperatures are deemed appropriate.

9.4.4 X-ray Absorption Near Edge Structure (XANES)

Figure 9.2 shows normalized XANES spectra of reference compounds (e.g., Co_3O_4, CoO, $CoAl_2O_4$, and Co^0 foil). A major characteristic of Co^0 is the edge peak at 7709 eV. In the oxide references, pre-edge features are associated with symmetry effects in the environment of cobalt and are due to $1s \rightarrow 3d$ transitions (Jacobs et al., 2007). The oxidic reference compounds (Co_3O_4, CoO, and $CoAl_2O_4$) display a stronger absorption white line with unique spectral features because cobalt atoms are in different Co-O environments and oxidation states. The pre-edge intensity of tetrahedral cobalt environments is stronger than that of octahedral cobalt environments (Bazin et al., 2000; Zayat et al., 2000). A pre-edge feature is observed in all oxide compounds. Co_3O_4 is a spinel structure, with one-third of the Co^{2+} occupying tetrahedral sites and two-thirds occupying octahedral sites ($2Co^{3+}$), such that the pre-edge feature represents a combination of the more intense tetrahedral peak and the weaker octahedral peak (Jacobs et al., 2007); CoO consists of Co^{2+}

octahedrally coordinated with oxygen (Jacobs et al., 2007; Saib et al., 2006);whereas and, $CoAl_2O_4$ is a normal spinel with Co^{2+} ions in tetrahedral sites (Saib et al., 2006; Zayat et al., 2000). Therefore, the intensity of pre-edge features follows the order: $CoAl_2O_4 > Co_3O_4 > CoO$. XANES spectra of supported CoO display a weak pre-edge feature. Moreover, the white line intensity and XANES shape are directly indicative of each cobalt oxide species. It is readily observed that the white line intensity in XANES spectra of supported CoO is higher than that of the CoO reference compound. This may be attributed to electron deficiencies due to a support effect (Jacobs et al., 2007). Hence, the white line in the catalyst spectrum will provide a good indication as to whether oxidation occurs in Co/Al_2O_3 at the onset of the FTS run mimicking 50% CO conversion.

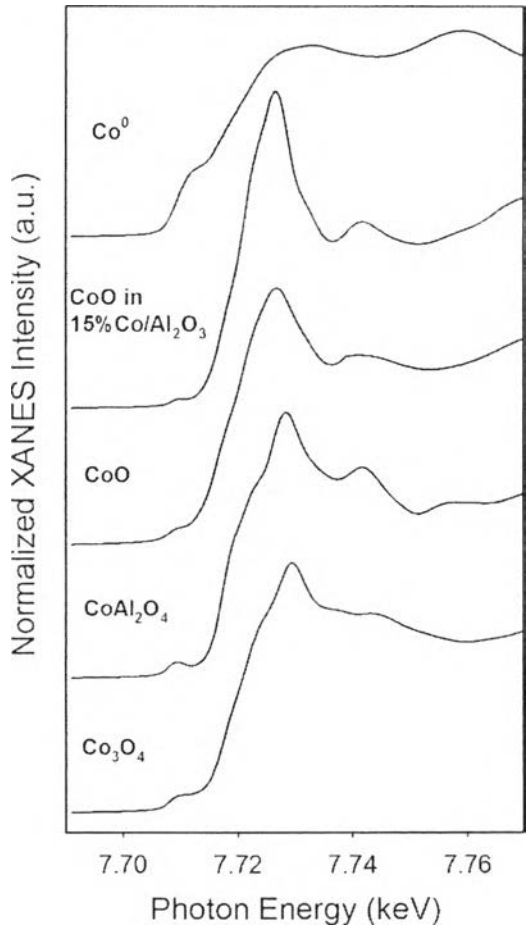

Figure 9.2 Normalized XANES spectra of reference compounds.

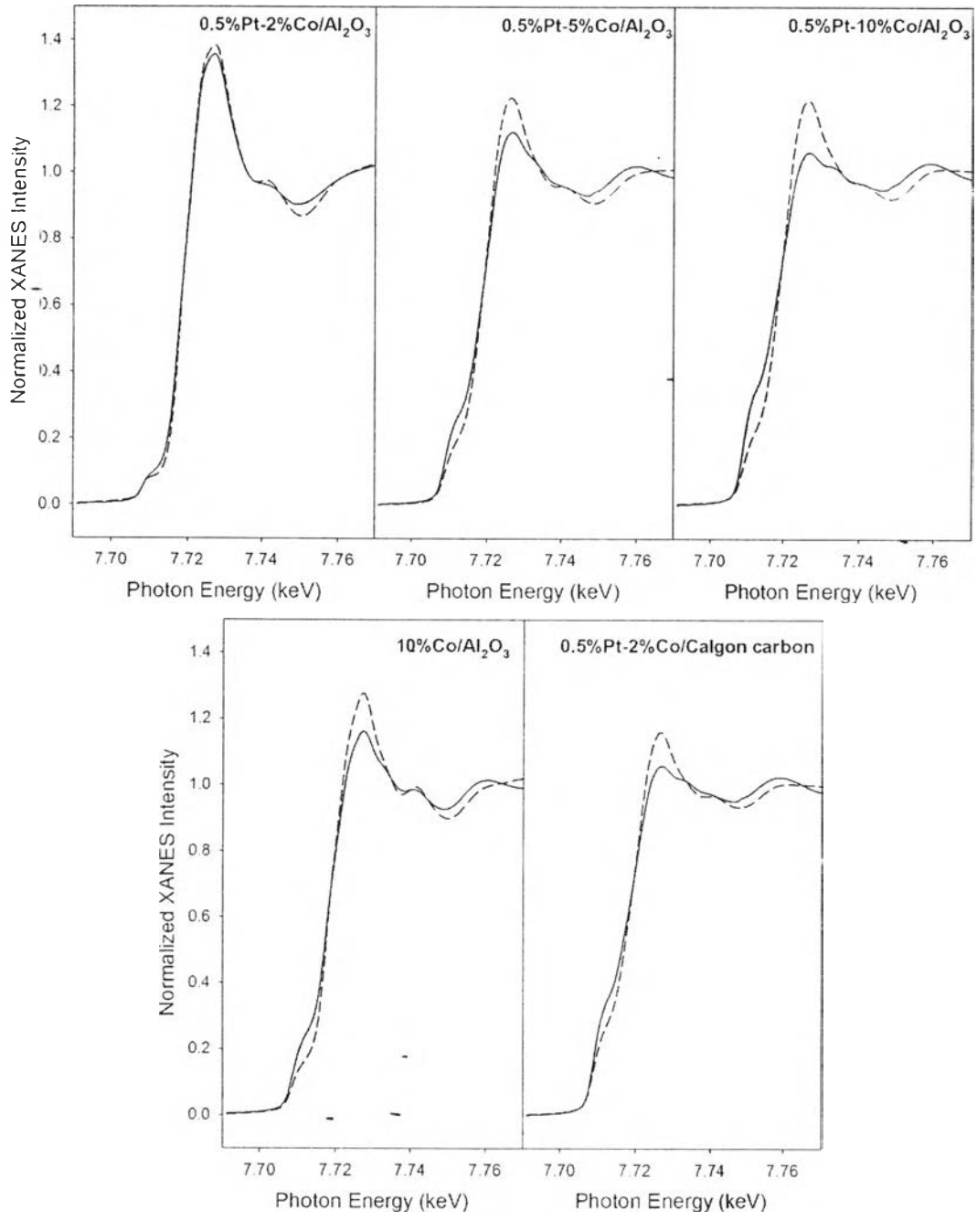

Figure 9.3 Comparative normalized XANES spectra of (solid line) reduced sample and (dashed line) FTS sample of Pt-Co/Al_2O_3, Co/Al_2O_3, and Pt-Co/Calgon carbon catalysts.

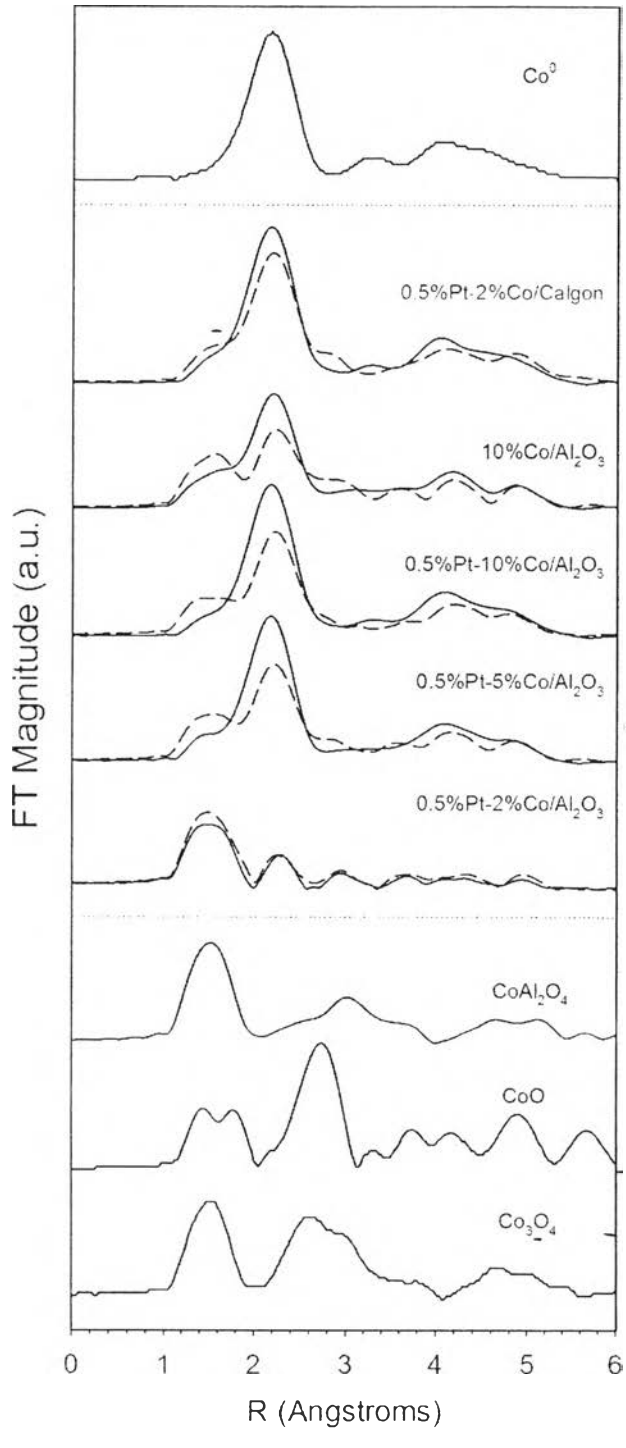

Figure 9.4 The k^1-Weighted Fourier transform magnitude of Co K-edge EXAFS spectra of reference compounds, catalyst samples after reduction (solid line), and catalyst samples after exposure to the onset of the FTS conditions mimicking 50% CO conversion (dashed line).

XANES measurements were performed for reduced and FTS samples of each catalyst to study whether nano-sized cobalt crystallites oxidize upon switching to FTS conditions. Figure 9.3 shows normalized XANES spectra of reduced and FTS samples of each catalyst, in which solid lines represent reduced catalysts while dashed lines show the results of FTS samples. The white line intensity of 0.5%Pt-2%Co/Al_2O_3 after exposure to FTS conditions is slightly higher than that of the reduced sample. It appears that there is little reduction during activation, while most of the cobalt oxides remain unreduced. This is consistent with the O_2 pulse reoxidation result that shows that only ~16% Co reduction is achieved with this catalyst. Moreover, a low peak intensity for Co^0 and an intense white line indicate low extent of reduction. Nevertheless, there is a small fraction of reduced Co that becomes oxidized as a slightly higher white line intensity is obtained during FTS. Moving to higher Co loading catalysts, 0.5%Pt-5%Co/Al_2O_3 and 0.5%Pt-10%Co/Al_2O_3, normalized XANES spectra reveal that cobalt in the reduced samples is mostly in metallic form. 10%Co does provide more Co metal than 5%Co, as a stronger edge peak for the metal is observed, along with a lower white line intensity. Following FTS conditions, a significant fraction of Co metal in these catalysts is oxidized and an increase in white line intensity with a decrease in the edge peak intensity for metallic cobalt is clearly observed. This reoxidation of Co metal into CoO at the onset of FTS is because the $H_2O/(H_2+CO)$ ratio is high enough to oxidize the smallest of the Co^0 crystallites (Hilmen et al., 1999; Van Berge et al., 2000; Van Steen et al., 2005) in the size distribution.

Comparing the activated Pt promoted and unpromoted 10%Co/Al_2O_3 catalysts, the white line is significantly lower for the Pt promoted catalyst. Reoxidation of Co metal in the unpromoted catalyst also occurred, but the difference is greater in the case of the Pt promoted catalyst. Since Pt facilitates the reduction of more strongly interacting CoO species, which tend to be smaller, it is not surprising that this higher density of smaller species would be more susceptible to reoxidation.

It is clear that Co metal dominates in the reduced sample of 0.5%Pt-2%Co/Calgon carbon; a comparison with the 0.5%Pt-2%Co/Al_2O_3 catalyst provides a testimony that less cobalt support compound formation occurs with the cobalt/carbon catalyst. 0.5%Pt-2%Co/Calgon carbon catalyst also exhibited

reoxidation of a fraction of Co^0 after switching to FTS conditions. A higher white line intensity in normalized XANES spectra and lower edge peak intensity for metallic Co^0 resulted after switching to FTS. Thus, small Co^0 crystallites of catalysts having supports that do not generally form significant fractions of cobalt support compounds can still undergo reoxidation.

9.4.5 Extended X-ray Absorption Fine Structure (EXAFS)

EXAFS results in Figure 9.4 are in agreement with the XANES results previously discussed. Qualitatively, in reduced samples (solid line), it is suggested that the peak of Co-O coordination appears as a minor shoulder to the Co-Co metal coordination peak in all catalysts, except 0.5%Pt-2%Co/Al_2O_3. The presence of Co-O bonding indicates that the reduced catalysts still contain a minor oxidized cobalt component (e.g., CoO). The dashed lines of Figure 9.4 represent the resulting EXAFS spectra after exposure to FTS conditions. Decreases in the peak associated with Co-Co coordination in the metal and increases in Co-O coordination are suggested. Moreover, Figure 9.5 also shows the results of the fitting using FEFFIT for the k^1-weighted EXAFS Fourier transform magnitude spectra and filtered k^1-weighted $\chi(k)$ spectra of supported Co catalysts. The solid lines in Figure 9.5 are the experimental data, while the circles provide the best fit. The results of fitting parameters are summarized in Table 9.2. Generally, the r-factor value of <0.02 indicates a good fit, and all catalyst spectra fall at or below this value. Qualitatively, the well-defined peak in the fitting corresponds to Co-Co bonding, while the shoulder peak is likely due primarily to Co-O bonding.

The EXAFS spectrum of 0.5%Pt-2%Co/Al_2O_3 reveals that Co-O coordination dominates in this catalyst even after reduction. After switching to FTS conditions, the peak tentatively assigned to Co-O appears to be slightly more intense. At higher Co loadings of 5% and 10%Co in Pt promoted Co/Al2O3 more pronounced Co-Co metal coordination peaks and less Co-O coordination is obtained, especially in the case of 0.5%Pt-10%Co/Al_2O_3, after activation. On the other hand, after FTS conditions, the peak ascribed to Co-Co metal coordination decreased with an apparent increase in Co-O coordination.

(A)

Co foil

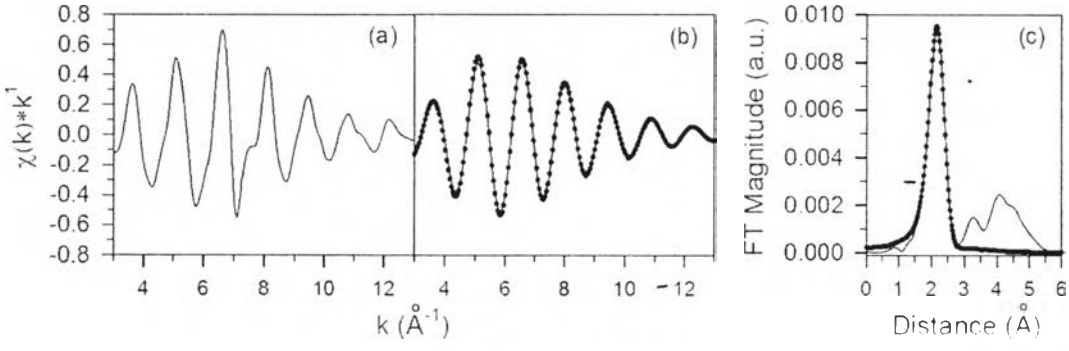

(B)

0.5%Pt-5%Co/Al_2O_3

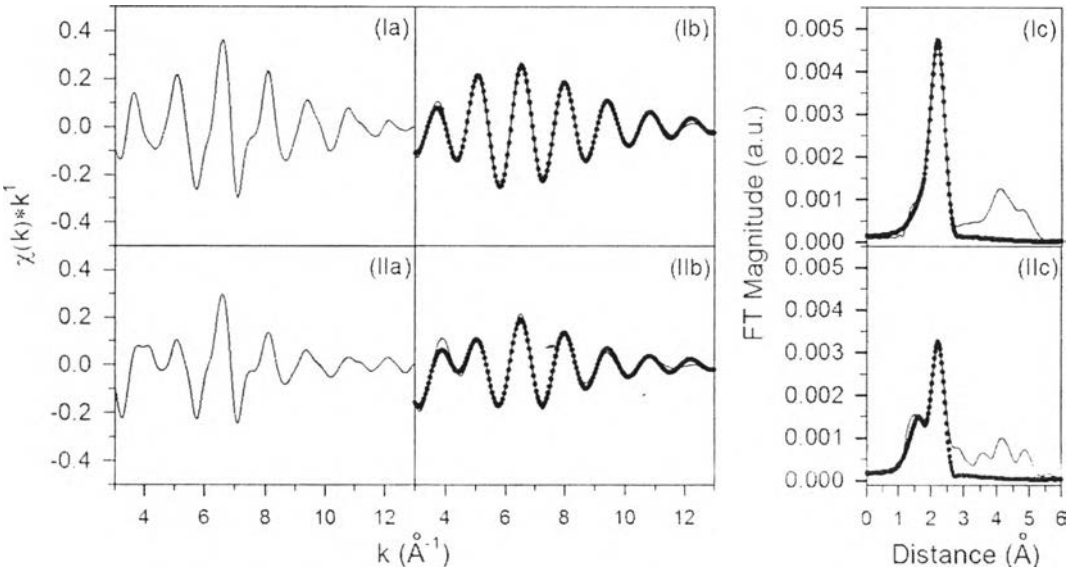

(C)

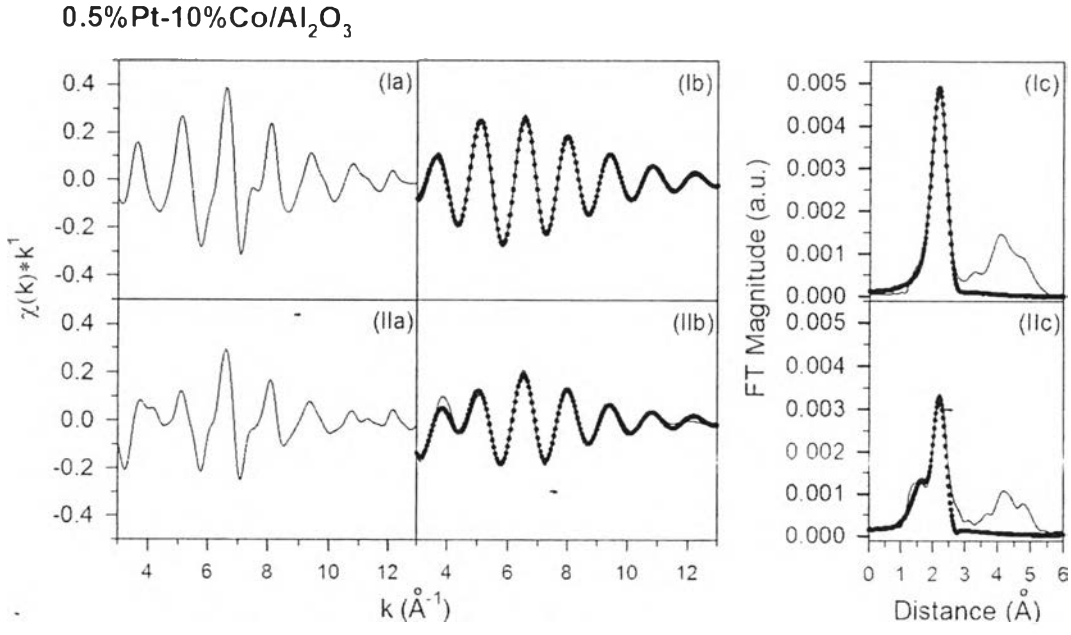
0.5%Pt-10%Co/Al2O3
(Ia)
(Ib)
(Ic)
(IIa)
(IIb)
(IIc)
χ(k)*k1
FT Magnitude (a.u.)
k (Å-1)
Distance (Å)

(D)

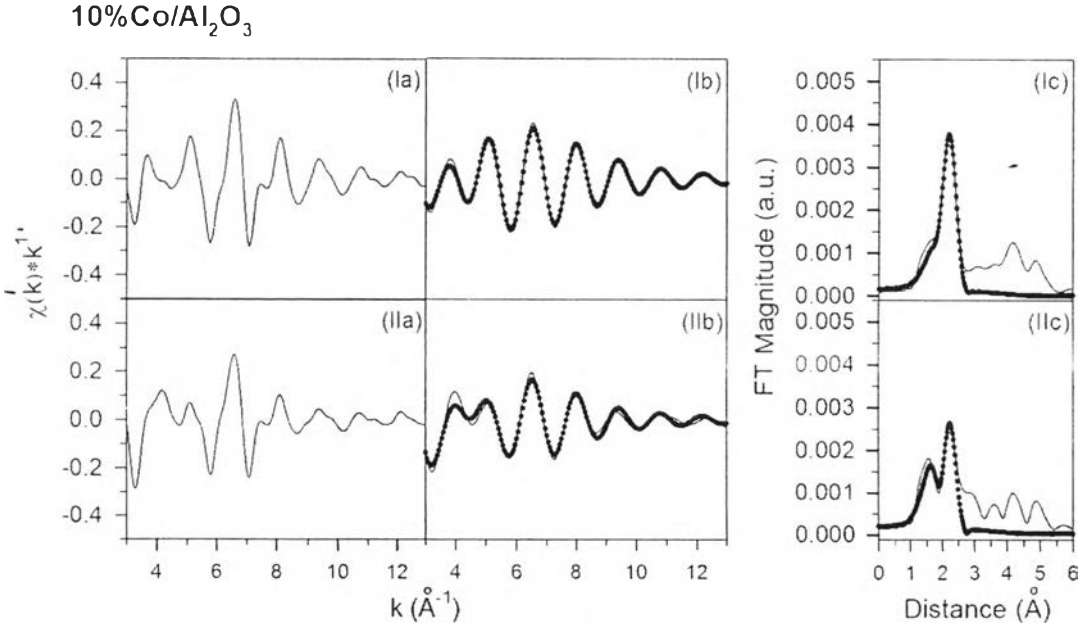
10%Co/Al2O3
(Ia)
(Ib)
(Ic)
(IIa)
(IIb)
(IIc)
χ(k)*k1
FT Magnitude (a.u.)
k (Å-1)
Distance (Å)

(E)

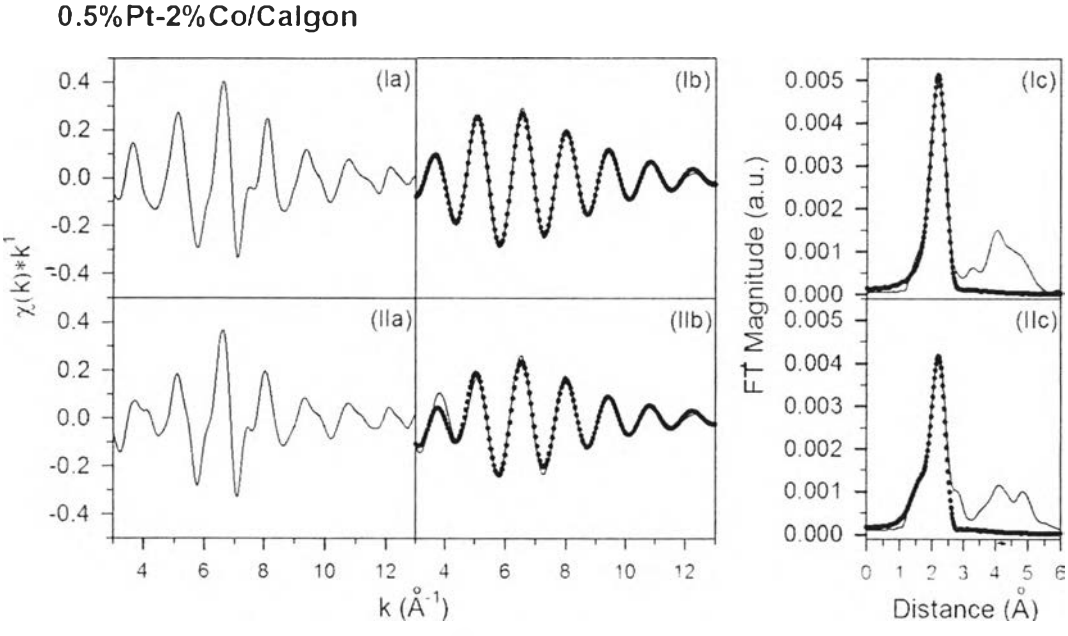

Figure 9.5 The results of EXAFS fittings: (a) unfiltered k^1-weighted $\chi(k)$ spectra; (b) filtered k^1-weighted $\chi(k)$ spectra (solid line) and resulting of fitting (filled circles); (c) k^1-weighted Fourier transform magnitude spectra (solid line) and resulting fitting (filled circles) over the first coordination shell of Co central atom, of (A) Co^0 foil reference and catalysts; (B) 0.5%Pt-5%Co/Al_2O_3, (C) 0.5%Pt-10%Co/Al_2O_3, (D) 10%Co/Al_2O_3, and (E) 0.5%Pt-2%Co/Calgon, at (I) after activation in H_2 and at (II) the onset of FTS at condition simulating 50% CO conversion.

To quantify the changes in coordination numbers and place the tentative peak assignments on a firmer footing, EXAFS fitting was performed by using the f.c.c. Co metal model and CoO as references (Figure 9.5(A)) with the assumption of Co-Co and Co-O first shell coordination being included in the fitting. Good fits were achieved, as shown in Figure 9.5 (B) and (C), with numeric fitting results being displayed in Table 9.2. It is observed that after reduction 0.5%Pt-10%Co/Al_2O_3 has a higher Co-Co coordination number than 0.5%Pt-5%Co/Al_2O_3 (5.80 vs 5.24), while after exposure to FTS conditions Co-O bond coordination was

higher for the 0.5%Pt-5%Co/Al_2O_3 catalyst (1.34 vs 1.55). It is suggested that the lower the Co loading, the more susceptible the smaller Co^0 particles are to reoxidation (i.e., in this case 3.4 vs 5.3 nm associated with 0.5%Pt-5%Co/Al_2O_3 and 0.5%Pt-10%Co/Al_2O_3 catalysts, respectively).

As expected, 10%Co/Al_2O_3 catalyst without Pt promoter contains more Co-O and less Co-Co coordination compared to 0.5%Pt-10%Co/Al_2O_3, as shown qualitatively in Figure 9.4 and Figure 9.5 (C) and (D) with fitting parameters quantified in Table 9.2. Considering the 0.5%Pt-2%Co/Calgon catalyst, which presumably formed less cobalt support complexes, Co-Co and Co-O coordination were close to those of the more highly loaded 0.5%Pt-10%Co/Al_2O_3 catalyst after activation, the latter support possessing a much stronger interaction with cobalt species, but containing a reduction promoter and a sufficiently high enough loading to achieve an adequate degree of reduction. The EXAFS results demonstrate that Co-Co metal coordination decreases while Co-O increases for all of the research catalysts upon exposure to FTS at useful conversions, indicating that a fraction of the small crystallites is readily oxidized after switching to FTS conditions. This is likely due to small cobalt crystallites (i.e., < 2 - 4.1 nm) present in the catalyst that, from the standpoint of thermodynamics, favor oxidation (Van Steen et al., 2005).

In the optimization of FT catalysts, researchers are now turning to novel supports (e.g., carbons (Bezemer et al., 2006), meso-porous sieves, etc.). Moreover, new preparation methods are being advanced (e.g., freeze-drying methods (Eggenhuisen et al., 2013)) aimed at generating a more uniform size distribution of cobalt nano-particles. Both procedures are aimed at making more efficient use of cobalt.

Utilizing the approach defined herein, XANES/EXAFS experiments would be useful in determining how sensitive the resulting cobalt particles are in these novel catalysts to oxidation at high conversion, and in defining the highest water partial pressures that the catalysts can sustain and still remain in the metallic state.

Table 9.2 Results of EXAFS fitting for data acquired near the Co K-edge for catalyst after activation and at the onset of FTS. The fitting ranges were approximately $\Delta k = 2\text{-}14$ Å^{-1} and $\Delta R = 1.25 - 2.7$ Å, $S_0^2 = 0.9$

Catalyst	Condition	$N_{Co\text{-}O}$	$R_{Co\text{-}O}$	$N_{Co\text{-}Co}$	$R_{Co\text{-}Co}$	e_0 (eV)	σ^2 (Å^2)	r-factor
Co^0 foil	-	-	-	12 (set)	2.486 (0.0063)	6.576 (0.772)	0.00665 (0.00047)	0.02
0.5%Pt-5%Co/Al_2O_3	Reduced	0.69 (0.11)	2.026 (0.0135)	5.24 (0.14)	2.495 (0.0037)	7.093 (0.460)	0.00538 (0.00057)	0.018
	FTS	1.55 (0.20)		3.53 (0.35)				
0.5%Pt-10%Co/Al_2O_3	Reduced	0.18 (0.08)	2.020 (0.0292)	5.80 (0.26)	2.495 (0.0030)	7.323 (0.375)	0.00600 (0.00044)	0.017
	FTS	1.34 (0.36)		3.83 (0.60)				
10%Co/Al_2O_3	Reduced	0.88 (0.11)	2.022 (0.0128)	4.48 (0.33)	2.503 (0.0044)	8.431 (0.498)	0.00603 (0.00073)	0.02
	FTS	1.75 (0.20)		3.08 (0.38)				
0.5%Pt-2%Co/Calgon carbon	Reduced	0.22 (0.11)	1.992 (0.0402)	5.76 (0.34)	2.493 (0.0040)	7.096 (0.510)	0.00554 (0.00058)	0.02
	FTS	0.97 (0.42)		4.71 (0.71)				

9.5 Conclusion

It is recognized that with FT research catalysts containing a low Co content with high Co dispersion, oxidation of a fraction of small Co crystallites occurs at the onset of FTS conditions at meaningful CO conversions. The small Co crystallites are susceptible to oxidation regardless of support type (i.e., even for Co supported on Calgon carbon, where cobalt support compounds are not a significant issue), as demonstrated by XANES/EXAFS results. This source of CoO, along with residual unreduced CoO following activation, likely contributes to a complex sintering mechanism involving agglomeration and net reduction of CoO, as well as Co aluminate formation (i.e., in the case of Co/alumina catalysts), during FTS as a function of time on-stream. Thus, small Co^0 crystallites should be avoided during preparation, as they contribute to catalyst deactivation. The techniques described will be useful in evaluating the susceptibility of new research catalysts to high conversion FTS conditions, and for establishing the highest water partial pressure that the catalysts can sustain and still remain in the active metallic state.

9.6 Acknowledgements

This work was sponsored by a NASA grant (Relating FTS catalyst properties to performance No.NNX11AI75A) and the commonwealth of Kentucky. This research was carried out, in part, at the National Synchrotron Light Source, Brookhaven National Laboratory, which is supported by the US DOE, Division of Materials Science and Chemical Science. We are also grateful to the Fulbright-Thailand Research Fund scholarship program for financial support for Mr. Thani Jermwongratanachai. Argonne's research was supported in part by the U.S. DOE, Office of Fossil Energy, NETL. The use of the APS was supported by the U.S. DOE, Office of Science, Office of Basic Energy Sciences, under Contract No. DE-AC02-06CH11357. MRCAT operations are supported by the DOE and the MRCAT member institutions.

9.7 References

Barrett, E.P., Joyner, L.G., and Halenda, P.P. (1951) The determination of pore volume and area distributions in porous substances. I. Computations from nitrogen isotherms. Journal of the American Chemical Society, 73(1), 373-380.

Bazin, D., Kovács, I., Guczi, L., Parent, P., Laffon, C., De Groot, F., Ducreux, O., and Lynch, J. (2000) Genesis of Co/SiO_2 catalysts: XAS study at the cobalt $L_{III,II}$ absorption edges. Journal of Catalysis, 189(2), 456-462.

Bezemer, G.L., Bitter, J.H., Kuipers, H.P.C.E., Oosterbeek, H., Holewijn, J.E., Xu, X., Kapteijn, F., van Dillen, A.J., and de Jong, K.P. (2006) Cobalt particle size effects in the Fischer–Tropsch reaction studied with carbon nanofiber supported catalysts. Journal of the American Chemical Society, 128(12), 3956-3964.

Brunauer, S., Emmett, P.H., and Teller, E. (1938) Adsorption of gases in multimolecular layers. Journal of the American Chemical Society, 60(2), 309-319.

Claeys, M., van Steen, E., Visagie, J., van de Loosdrecht, J. (2011, June) Characterization of Fischer-Tropsch catalysts using a novel in-situ magnetometer. Paper presented at 22nd Meeting of the North American Catalysis Society, Detroit, USA.

Das, T.K., Jacobs, G., Patterson, P.M., Conner, W.A., Li, J., and Davis, B.H. (2003) Fischer–Tropsch synthesis: characterization and catalytic properties of rhenium promoted cobalt alumina catalysts. Fuel, 82(7), 805-815.

Eggenhuisen, T.M., Munnik, P., Talsma, H., de Jongh, P.E., and de Jong, K.P. (2013) Freeze-drying for controlled nanoparticle distribution in Co/SiO_2 Fischer–Tropsch catalysts. Journal of Catalysis, 297, 306-313.

Feltes, T., Fischer, N., and Claeys, M. (2013, March) The reversibility of the size dependent re-oxidation of a Co/Al_2O_3 Fischer-Tropsch catalyst by in-situ magnetic measurements. Paper presented at 10th Natural Gas Conversion Symposium, Doha, Qatar.

Fischer, N., Clapham, B., Feltes, T.E., van Steen, E., and Claeys, M. (2012, April) The reoxidation of cobalt Fischer-Tropsch catalysts. Paper presented at 2012 Syngas Convention, Cape Town, South Africa.

Guczi, L., Bazin, D., Kovács, I., Borkó, L., Schay, Z., Lynch, J., Parent, P., Lafon, C., Stefler, G., Koppány, Z., and Sajó, I. (2002) Structure of Pt–Co/Al_2O_3 and Pt–Co/NaY bimetallic catalysts: Characterization by in situ EXAFS, TPR, XPS and by activity in Co (carbon monoxide) hydrogenation. Topics in Catalysis, 20(1-4), 129-139.

Hilmen, A.M., Schanke, D., Hanssen, K.F., and Holmen, A. (1999) Study of the effect of water on alumina supported cobalt Fischer–Tropsch catalysts. Applied Catalysis A: General, 186(1–2), 169-188.

Jacobs, G., Chaney, J.A., Patterson, P.M., Das, T.K., Maillot, J.C., and Davis, B.H. (2004) Fischer-Tropsch synthesis: study of the promotion of Pt on the reduction property of Co/Al_2O_3 catalysts by in situ EXAFS of Co K and Pt L_{III} edges and XPS. Journal of Synchrotron Radiation, 11(5), 414-422.

Jacobs, G., Das, T.K., Patterson, P.M., Li, J., Sanchez, L., and Davis, B.H. (2003) Fischer–Tropsch synthesis XAFS: XAFS studies of the effect of water on a Pt-promoted Co/Al_2O_3 catalyst. Applied Catalysis A: General, 247(2), 335-343.

Jacobs, G., Das, T.K., Zhang, Y., Li, J., Racoillet, G., and Davis, B.H. (2002) Fischer–Tropsch synthesis: support, loading, and promoter effects on the reducibility of cobalt catalysts. Applied Catalysis A: General, 233(1–2), 263-281.

Jacobs, G., Ji, Y., Davis, B.H., Cronauer, D., Kropf, A.J., and Marshall, C.L. (2007) Fischer–Tropsch synthesis: Temperature programmed EXAFS/XANES investigation of the influence of support type, cobalt loading, and noble metal promoter addition to the reduction behavior of cobalt oxide particles. Applied Catalysis A: General, 333(2), 177-191.

Jacobs, G., Patterson, P.M., Das, T.K., Luo, M., and Davis, B.H. (2004) Fischer–Tropsch synthesis: effect of water on Co/Al_2O_3 catalysts and XAFS characterization of reoxidation phenomena. Applied Catalysis A: General, 270(1–2), 65-76.

Jacobs, G., Patterson, P.M., Zhang, Y., Das, T., Li, J., and Davis, B.H. (2002) Fischer–Tropsch synthesis: deactivation of noble metal-promoted Co/Al_2O_3 catalysts. Applied Catalysis A: General, 233(1–2), 215-226.

Jacobs, G., Sarkar, A., Ji, Y., Patterson, P.M., Das, T.K., Luo, M., and Davis, B.H. (2006, November) Fischer-Tropsch synthesis: Characterization of interactions between reduction promoters and Co for Co/Al_2O_3–based GTL catalysts. Paper presented at 2006 AIChE Annual Meeting. San Francisco, California, USA.

Li, J., Jacobs, G., Das, T., Zhang, Y., and Davis, B. (2002) Fischer–Tropsch synthesis: effect of water on the catalytic properties of a Co/SiO_2 catalyst. Applied Catalysis A: General, 236(1–2), 67-76.

Li, J., Zhan, X., Zhang, Y., Jacobs, G., Das, T., and Davis, B.H. (2002) Fischer–Tropsch synthesis: effect of water on the deactivation of Pt promoted Co/Al_2O_3 catalysts. Applied Catalysis A: General, 228(1–2), 203-212.

Ma, W., Jacobs, G., Ji, Y., Bhatelia, T., Bukur, D., Khalid, S., and Davis, B. (2011) Fischer–Tropsch synthesis: Influence of CO conversion on selectivities, H_2/CO usage ratios, and catalyst stability for a Ru promoted Co/Al_2O_3 catalyst using a slurry phase reactor. Topics in Catalysis, 54(13-15), 757-767.

Moodley, D.J., Saib, A.M., van de Loosdrecht, J., Welker-Nieuwoudt, C.A., Sigwebela, B.H., and Niemantsverdriet, J.W. (2011) The impact of cobalt aluminate formation on the deactivation of cobalt-based Fischer–Tropsch synthesis catalysts. Catalysis Today, 171(1), 192-200.

Rønning, M., Tsakoumis, N.E., Voronov, A., Johnsen, R.E., Norby, P., van Beek, W., Borg, Ø., Rytter, E., and Holmen, A. (2010) Combined XRD and XANES studies of a Re-promoted $Co/\gamma\text{-}Al_2O_3$ catalyst at Fischer–Tropsch synthesis conditions. Catalysis Today, 155(3–4), 289-295.

Saib, A.M., Borgna, A., van de Loosdrecht, J., van Berge, P.J., and Niemantsverdriet, J.W. (2006) XANES study of the susceptibility of nano-sized cobalt crystallites to oxidation during realistic Fischer–Tropsch synthesis. Applied Catalysis A: General, 312, 12-19.

Saib, A.M., Moodley, D.J., Ciobîcă, I.M., Hauman, M.M., Sigwebela, B.H., Weststrate, C.J., Niemantsverdriet, J.W., and van de Loosdrecht, J. (2010) Fundamental understanding of deactivation and regeneration of cobalt Fischer–Tropsch synthesis catalysts. Catalysis Today, 154(3–4), 271-282.

Sirijaruphan, A., Horváth, A., Goodwin Jr, J.G., and Oukaci, R. (2003) Cobalt aluminate formation in alumina-supported cobalt catalysts: Effects of cobalt reduction state and water vapor. Catalysis Letters, 91(1-2), 89-94.

Storsater, S., Borg, O., Blekkan, E., and Holmen, A. (2005) Study of the effect of water on Fischer–Tropsch synthesis over supported cobalt catalysts. Journal of Catalysis, 231(2), 405-419.

Tsakoumis, N.E., Rønning, M., Borg, Ø., Rytter, E., and Holmen, A. (2010) Deactivation of cobalt based Fischer–Tropsch catalysts: A review. Catalysis Today, 154(3–4), 162-182.

Van Berge, P.J., van de Loosdrecht, J., Barradas, S., and van der Kraan, A.M. (2000) Oxidation of cobalt based Fischer–Tropsch catalysts as a deactivation mechanism. Catalysis Today, 58(4), 321-334.

Van de Loosdrecht, J., Balzhinimaev, B., Dalmon, J.A., Niemantsverdriet, J.W., Tsybulya, S.V., Saib, A.M., van Berge, P.J., and Visagie, J.L. (2007) Cobalt Fischer-Tropsch synthesis: Deactivation by oxidation? Catalysis Today, 123(1–4), 293-302.

Van Steen, E., Claeys, M., Dry, M.E., Van De Loosdrecht, J., Viljoen, E.L., and Visagie, J.L. (2005) Stability of nanocrystals: Thermodynamic analysis of oxidation and re-reduction of cobalt in water/hydrogen mixtures. Journal of Physical Chemistry B, 109(8), 3575-3577.

Wang, W.J. and Chen, Y.-W. (1991) Influence of metal loading on the reducibility and hydrogenation activity of cobalt/alumina catalysts. Applied Catalysis, 77(2), 223-233.

Zayat, M. and Levy, D. (2000) Blue $CoAl_2O_4$ particles prepared by the sol-gel and citrate-gel methods. Chemistry of Materials, 12(9), 2763-2769.